

ARCHIMEDEAN-TYPE FORCE IN A COSMIC DARK FLUID: II. QUALITATIVE AND NUMERICAL STUDY OF A MULTISTAGE UNIVERSE EXPANSION

Alexander B. Balakin and Vladimir V. Bochkarev
Kazan Federal University, Kazan, Russia
(Dated: February 7, 2011)

In this (second) part of the work we present the results of numerical and qualitative analysis, based on a new model of the Archimedean-type interaction between dark matter and dark energy. The Archimedean-type force is linear in the four-gradient of the dark energy pressure and plays a role of self-regulator of the energy redistribution in a cosmic dark fluid. Because of the Archimedean-type interaction the cosmological evolution is shown to have a multistage character. Depending on the choice of the values of the model guiding parameters, the Universe's expansion is shown to be perpetually accelerated, periodic or quasiperiodic with finite number of deceleration/acceleration epochs. We distinguished the models, which can be definitely characterized by the inflation in the early Universe, by the late-time accelerated expansion and nonsingular behavior in intermediate epochs, and classified them with respect to a number of transition points. Transition points appear, when the acceleration parameter changes the sign, providing the natural partition of the Universe's history into epochs of accelerated and decelerated expansion. The strategy and results of numerical calculations are advocated by the qualitative analysis of the instantaneous phase portraits of the dynamic system associated with the key equation for the dark energy pressure evolution.

I. INTRODUCTION

The concepts of dark energy (DE) and dark matter (DM) [1]-[6] considered as two manifestations of one unified dark fluid [7]-[12] are basic elements of modern cosmology and astrophysics. Because the dark fluid is estimated to accumulate about 95% of the Universe's energy, the coupling of DE with DM predestine the main features of the Universe evolution. In the first part of the work [13] we introduced the so-called Archimedean-type force, which is linear in the four-gradient of the DE pressure and acts on the DM particles. This force is a relativistic generalization of the classical Archimedean force and belongs to the class of effective forces described in [14]-[19]. From mathematical point of view the presented model gives us a new self-consistent nonlinear scheme of interaction between two constituents of the cosmic medium. From physical point of view the Archimedean-type force is an effective redistributor of the total energy of the Universe between the DE and DM constituents. The Archimedean-type model can be also considered in terms of two-fluid representation of the cosmic medium [20]-[25], in which the interaction terms $\pm Q$ appear in the right-hand sides of separate balance equations for the DE and DM with opposite signs and which disappear in a sum, when one deals with the total balance equation. We formulated in [13] the theory of interaction between DE and DM by using the relativistic hydrodynamics for dark energy and relativistic kinetics for dark matter.

In the first paper [13] we focused on the submodels with some special values of guiding parameters, which admit exact analytical solutions of the total self-consistent system of master equations; in particular, we discussed the so-called anti-Gaussian solution. Now we consider the results of numerical and qualitative analysis for all admissible sets of guiding parameters and initial data.

This paper is organized as follows. In Sec.II we recall briefly the key equations and basic formulas of the model with Archimedean-type coupling between dark energy and dark matter. In Sec.III the numerical results are presented: in Sec.III A we explain the scheme of numerical analysis and details of results representation; in Sec.III B we classify the models using the number of transition points and discuss details of seven submodels, the perpetually accelerated and periodic universes being among them. In Sec.IV we analyze the model of Archimedean-type coupling in terms of dynamic system associated with nonlinear key equation for the DE pressure; in Sec.IV A we study the toy model, which relates to the autonomous dynamic system, find critical points and discuss two basic phase portraits of this system; in Sec.IV B we analyze instantaneous phase portraits of a general nonautonomous dynamic system in the context of numerical results presented in Sec.III; in Sec.IV C we consider asymptotical behavior of the models. Sec.V contains discussions: in Sec.V A we attract an attention to the inflationary behavior of the model in the early Universe; in Sec.V B we show that all the models under discussion manifest the late-time accelerated expansion; in Sec.V.C we touch on the coincidence problem.

II. MASTER EQUATIONS OF THE TOY MODEL

A. Dynamic parameters of the Universe

In order to describe the Universe's evolution from the dynamic point of view, we find three key functions: the scale factor $a(t)$, the Hubble function $H(t)$ and the acceleration parameter $-q(t)$ given by the standard defini-

tions,

$$H(t) \equiv \frac{\dot{a}(t)}{a(t)}, \quad -q(t) \equiv \frac{\ddot{a}(t)}{a(t)H^2(t)}. \quad (1)$$

The space-time is considered to be of the spatially homogeneous Friedmann-Lemaître-Robertson-Walker (FLRW) type with the metric

$$ds^2 = dt^2 - a^2(t)[(dx^1)^2 + (dx^2)^2 + (dx^3)^2]. \quad (2)$$

When all the functions describing the state of the Universe, $\mathcal{S}(t)$, depend on time through the scale factor $\mathcal{S}[a(t)]$, it is convenient to use the new variable x and the following relations, associated with x :

$$x \equiv \frac{a(t)}{a(t_0)}, \quad \frac{d}{dt} = xH(x)\frac{d}{dx}, \quad t-t_0 = \int_0^{\frac{a(t)}{a(t_0)}} \frac{dx}{xH(x)}. \quad (3)$$

The last equality gives the scale factor $a(t)$, when $H(x)$ is found from the Einstein equations, which can be written in the form

$$x \frac{d}{dx} H^2(x) = -8\pi G[\rho(x) + E(x) + \Pi(x) + P(x)], \quad (4)$$

$$H^2 = \frac{8\pi G}{3}(\rho + E). \quad (5)$$

The quantities in the right-hand sides of the Einstein equations are interpreted as follows: ρ is the energy density of the dark energy and Π is its pressure; E and P are, respectively, the total energy density and the total pressure of the dark matter. In these terms the acceleration parameter $-q$ can also be represented as

$$-q(x) = 1 + x \frac{d}{dx} \log H(x) = -\frac{1}{2} \left[1 + 3 \left(\frac{\Pi + P}{\rho + E} \right) (x) \right]. \quad (6)$$

B. Balance equations

It was shown in the first part of our work that the separate equations of the energy balance for the DM and DE constituents of the dark fluid can be presented in the form

$$x \frac{d}{dx} E(x) + 3(E + P) = -\mathcal{Q}(x), \quad (7)$$

$$x \frac{d}{dx} \rho(x) + 3(\rho + \Pi) = \mathcal{Q}(x). \quad (8)$$

The total system (DE plus DM) is considered to be conserved, the sum of (7) and (8) yields the total balance equation

$$x \frac{d}{dx} [\rho(x) + E(x)] + 3(\rho + E + \Pi + P) = 0, \quad (9)$$

which is, clearly, the compatibility condition for the pair of equations (4) and (5). The source term \mathcal{Q} , which was introduced in the first part of our work, has the form

$$\mathcal{Q} \equiv 3x \left[\frac{d}{dx} \Pi(x) \right] \sum_{(a)} \mathcal{V}_{(a)} P_{(a)}(x), \quad (10)$$

where $P_{(a)}$ is a partial pressure of the DM particles of the sort (a) and $\mathcal{V}_{(a)}$ is the guiding parameter associated with the Archimedean-type force.

The DE energy density ρ and DE pressure Π are coupled by the linear inhomogeneous equation of state [26]-[31]

$$\rho(x) = \rho_0 + \sigma \Pi(x) + \xi x \frac{d}{dx} \Pi(x). \quad (11)$$

The state functions $E(x)$ and $P(x)$, which characterize the DM constituent, are presented by the integrals

$$E(x) = \sum_{(a)} \frac{E_{(a)}}{x^3} \int_0^\infty q^2 dq \sqrt{1+q^2 F_{(a)}(x)} e^{-\lambda_{(a)} \sqrt{1+q^2}}, \quad (12)$$

$$P(x) = \sum_{(a)} \frac{E_{(a)}}{3x^3} \int_0^\infty \frac{F_{(a)}(x) q^4 dq}{\sqrt{1+q^2 F_{(a)}(x)}} e^{-\lambda_{(a)} \sqrt{1+q^2}}, \quad (13)$$

where the following auxiliary quantities are introduced

$$F_{(a)}(x) = \frac{1}{x^2} \exp \{ 2\mathcal{V}_{(a)} [\Pi(1) - \Pi(x)] \}, \quad (14)$$

$$E_{(a)} \equiv \frac{N_{(a)} m_{(a)} \lambda_{(a)}}{K_2(\lambda_{(a)})}, \quad \lambda_{(a)} \equiv \frac{m_{(a)}}{k_{(B)} T_{(a)}}, \quad (15)$$

$$K_\nu(\lambda_{(a)}) \equiv \int_0^\infty dz \cosh \nu z \cdot \exp [-\lambda_{(a)} \cosh z]. \quad (16)$$

Here $K_2(\lambda_{(a)})$ is the modified Bessel function, $k_{(B)}$ is the Boltzmann constant, and $T_{(a)}$ is the partial temperature of the particles of the sort (a) [32, 33].

C. Key equation of the toy model

Clearly, the key element of the toy model is the function $\Pi(x)$; to find the DE pressure $\Pi(x)$ we use the key equation

$$\xi x^2 \Pi''(x) + x \Pi'(x) (4\xi + \sigma) + 3(1 + \sigma) \Pi + 3\rho_0 = \mathcal{J}(x), \quad (17)$$

where the prime denotes the derivative with respect to x . The source term $\mathcal{J}(x) = \mathcal{J}(x, \Pi - \Pi(1), \Pi')$ is generally presented by the integral

$$\mathcal{J}(x) = - \sum_{(a)} E_{(a)} \frac{[x^2 F_{(a)}(x)]'}{2x^4} \int_0^\infty \frac{q^4 dq e^{-\lambda_{(a)} \sqrt{1+q^2}}}{\sqrt{1+q^2 F_{(a)}(x)}}, \quad (18)$$

and we use them for numerical calculations. For the qualitative analysis we use the explicit model expression for the source term

$$\mathcal{J}_*(x) = E_* \mathcal{V}_* \frac{\Pi'(x)}{x^\mu} \exp \{ \mathcal{V}_* [\Pi(1) - \Pi(x)] \}. \quad (19)$$

Here $\Pi(1)$ denotes the initial value for the DE pressure (let us remind that $\Pi(x=1) = \Pi[a(t=t_0)]$). When we deal with massless particles, the corresponding source term coincides with (19), if

$$\mu = 3, \quad E_* = E_{(0)}, \quad \mathcal{V}_* = \mathcal{V}_{(0)}. \quad (20)$$

When we deal with the cold dark matter, we use the source term (19) with

$$\mu = 4, \quad E_* = \frac{3N_{(C)}}{k_{(B)}T_{(C)}}, \quad \mathcal{V}_* = 2\mathcal{V}_{(C)}. \quad (21)$$

Thus, the key equation (17) is the ordinary differential equation of the second order linear in the derivatives of the unknown function $\Pi''(x)$, $\Pi'(x)$ and nonlinear in the function $\Pi(x)$ itself.

Let us mention that, when $\sigma \neq -1$, the effective guiding parameter ρ_0^* can be introduced instead of ρ_0 . Indeed, using a new unknown function $\pi(x) \equiv \Pi(x) - \Pi(1)$ one can rewrite the key equation (17) in the form

$$\xi x^2 \pi''(x) + x \pi'(x) (4\xi + \sigma) + 3(1 + \sigma)\pi + 3\rho_0^* = \mathcal{J}(x, \pi, \pi'), \quad (22)$$

where

$$\rho_0^* = \rho_0 + (1 + \sigma)\Pi(1). \quad (23)$$

Clearly, the parameters ρ_0^* and ρ_0 coincide at $\sigma = -1$.

III. NUMERICAL RESULTS

A. About the scheme of analysis

We analyze the Archimedean-type model as follows. First, we integrate the key equation (17) with the source term (18) and find the DE pressure $\Pi(x)$. Then we calculate the function $\rho(x)$ using (11), the functions $E(x)$ and $P(x)$ using (12) and (13), respectively, then we find the Hubble function $H(x)$ using (5), the acceleration parameter $-q(x)$ using (6) and finally the scale factor $a(t)$ using (3). Let us make seven remarks about the scheme of numerical analysis.

1. The solution for the DE pressure $\Pi(x)$ depends on the following guiding parameters: ξ , σ , ρ_0^* , $\mathcal{V}_{(a)}$, $E_{(a)}$, $\lambda_{(a)}$ and on two initial values $\Pi(1)$, $\Pi'(1)$. We fulfilled systematic numerical calculations by varying one of these parameters and fixing the remaining ones, and then we classified the obtained plots picking out principally different classes of solutions. For the numerical analysis we used two-component DM model, one component being

massless (ultrarelativistic), another one being cold (non-relativistic). Nevertheless, in order to illustrate the main details of the Universe expansion on the plots we considered only one (leading) component of the DM. Below we summarize the results, emphasize the main features, but do not discuss details of numerical calculations.

2. For a number of sets of the guiding parameters and initial data, mentioned above, the behavior of the solution is of a singular type, i.e., the scale factor, Hubble function, or/and DE pressure, DE energy, etc., can take infinite values at a finite time moment $t=t_{(s)} > t_0$; we do not discuss such solutions here.

3. We omit the discussion of submodels for which the DM energy density and DM pressure grow infinitely at $t \rightarrow \infty$ or tend to finite (nonvanishing) asymptotic values. In other words, we restrict ourselves by the submodels, for which the DE component dominates over DM starting from definite time moment; this motive explains why we consider the parameters $E_{(a)}(t_0)$ to be unchanged in the presented plots.

4. There exist a lot of sets of the guiding parameters for which the solutions for the DE energy and DE pressure are asymptotically unstable; we do not focus on them here.

5. We discuss only the solutions for which the total energy $\rho + E$ is non-negative for arbitrary t , thus guaranteeing that H is a real function [see (5)].

6. In order to describe the Archimedean-type model completely we have to indicate the domain in the multidimensional space of parameters ξ , σ , ρ_0 , $\mathcal{V}_{(a)}$, $E_{(a)}$, $\lambda_{(a)}$, $\Pi(1)$ and $\Pi'(1)$ in which the solutions are nonsingular and asymptotically stable; we hope to solve this problem in a special paper and do not discuss them here.

7. Figures 1-7 present the results of numerical calculations and are organized as follows. In the first panels labeled (a) [$1 \leq N \leq 7$] the plot of the DE energy $\rho(\tau)$ is presented; (b) contains the plot of the DM energy density $E(\tau)$; the DE pressure $\Pi(\tau)$ and DM pressure $P(\tau)$ are presented in panels (c) and (d), respectively; the plot of the Hubble function $H(\tau)$ can be found in panels (e); the acceleration parameter $-q(\tau)$ is placed in (f), and finally, the plots of the scale factor $a(t)$ are given in (g). Let us remind, that the parameter $\tau \equiv \log x = \log \frac{a(t)}{a(t_0)}$ specifies the logarithmic scale in figure panels (a)-(f), and the value $\tau=0$ corresponds to $t=t_0$; the plots in panels (g) are presented in terms of logarithm of the normalized cosmological time t/t_0 .

B. Multistage character of the Universe's evolution

The analysis of the pictures presented in Figs.1(f),2(f),3(f),4(f),5(f),6(f), and 7(f) shows explicitly that for a wide choice of sets of the parameters ξ , σ , ρ_0 , $\mathcal{V}_{(a)}$, $E_{(a)}$, $\lambda_{(a)}$, $\Pi(1)$ and $\Pi'(1)$ the function $-q(\tau)$ is not monotonic and can change the sign. We indicate the points, in which the function $-q(\tau)$ changes the sign, as *transition* points, which divide the history

of the Universe into deceleration/acceleration *epochs*; we denote these points as $\tau_{(\text{trans})}^{(k)}$. The epochs with accelerated expansion can give way to the epochs with deceleration, the number of changes being finite or infinite. When the (continuous) curve $-q(\tau)$ has *extrema*, it is natural to divide the corresponding epochs into *eras*, the number of eras relates to the number of maximums and minimums. Thus, depending on the number of transition points (related to the number of (simple) roots of the equation $q(\tau) = 0$), we divide below all the models into three classes and into a number of sub-classes.

1. Perpetually accelerated universe (no transition points)

The first class of models relates to the case when the function $-q(\tau)$ is non-negative for $\tau \geq 0$. In [13] we discussed the so-called anti-Gaussian model: exact solutions in this model were presented in terms of elementary functions at $\sigma = -1$. In particular, the acceleration parameter obtained there, $-q(t) = 1 + \frac{3V_{(0)}}{16\pi G(t-t^*)^2}$, is a monotonic positively defined function exceeding the value $-q_{(\text{dS})} = 1$, the acceleration parameter for the de Sitter models. In other words, there are no transition points, there is no splitting of the history into epochs and eras, when we deal with an anti-Gaussian universe. Another example presented in [13] describes superexponential expansion with the acceleration parameter given by $-q(t) = 1 + \sqrt{\frac{9\rho_0}{2\rho(1)}} \frac{\sinh\left[\frac{\sqrt{12\pi G\rho_0}(t-t_0)}{\sqrt{12\pi G\rho_0}(t-t_0)}\right]}{\cosh^2\left[\frac{\sqrt{12\pi G\rho_0}(t-t_0)}{\sqrt{12\pi G\rho_0}(t-t_0)}\right]}$. The plot of this function starts with $-q(t_0) = 1$, reaches the maximum $-q_{(\text{max})} = 1 + \sqrt{\frac{9\rho_0}{8\rho(1)}}$ at $t = t_0 + \frac{\log(1+\sqrt{2})}{\sqrt{12\pi G\rho_0}}$, and tends asymptotically to $-q(\infty) = 1$. In the context of our terminology, we also deal with perpetually accelerated universe, but its history is now divided into two eras. Here we discuss an alternative example of a perpetually accelerated universe with $\sigma \neq -1$, studied numerically. Typical pictures illustrating this class of models are given in Fig.1.

The solid curve in Fig.1(f) touches the line $q = 0$ in one point, other curves lie above $q = 0$, thus there are no transition points. In this class of models the acceleration parameter $-q$ as a function of time is non-negative for arbitrary τ : this means that the accelerated expansion of the Universe is perpetual. For the model under discussion the DE energy density ρ is (perpetually) non-negative [see Fig.1(a)], the DE pressure Π is nonpositive. The acceleration parameter, the DE energy density and pressure, and the Hubble function change nonmonotonically with time, thus, the statefinder parameter $r \equiv \frac{1}{aH^3} \frac{d^3 a}{dt^3}$, introduced in [34], is necessary to describe the details of the Universe's evolution. We do not focus now on these fine details of the model and their physical interpretation, nevertheless, we have to stress, that extrema of the function $-q(\tau)$ divide naturally the history of the

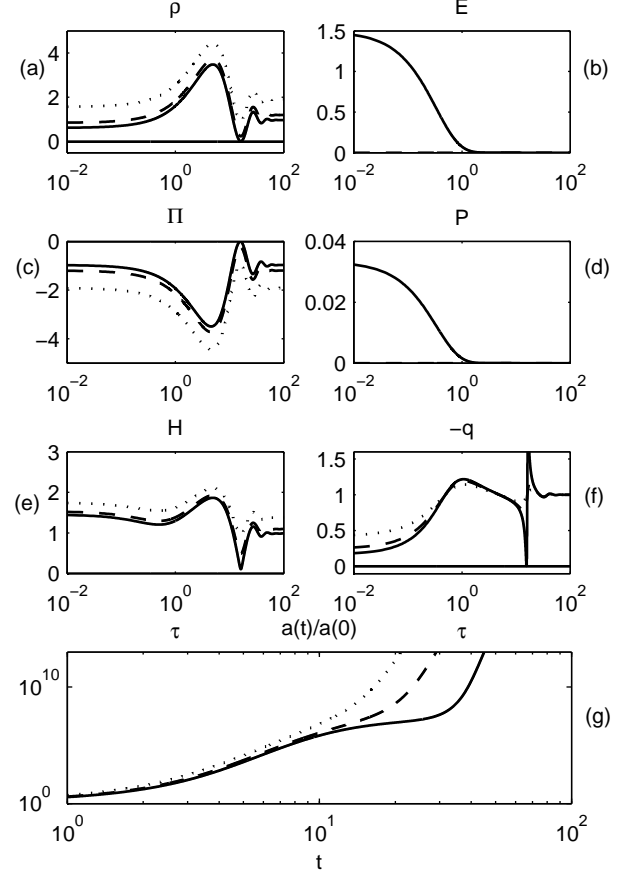


FIG. 1. Perpetually accelerated universe: the acceleration parameter $-q(\tau)$ is non-negative for arbitrary τ . Since there are no transition points, in which $-q(\tau)$ changes the sign, the history of this universe includes only one epoch; since at least five extrema can be recognized in Fig.1(f), the history consists of six or more eras. Here the dark solid line relates to the following set of the parameters: $\xi = 0.35$, $\sigma = -0.99$ (i.e., $3\xi + \sigma \simeq 0.06 > 0$), $V_{(0)} = 1$, $E_{(0)} = 0.0205$, $\lambda_{(0)} = 1$ (i.e., the DM is initially medium-relativistic), $\rho_* = 0.333 \cdot 10^{-4}$, and $\Pi'(1) = -1$.

Universe into the corresponding eras, thus describing the multistage character of its evolution.

The history of a perpetually accelerated universe includes only one epoch, but consists at least of six eras. Indeed, one can clearly identify at least three maximums and two minimums of the curve $-q(\tau)$ which divide the acceleration epoch into six eras. The first era ($\tau < 10^0$) can be indicated as the era of a first superacceleration. During this era the DE energy - density, $\rho(\tau)$, grows monotonically [see Fig.1(a)], the DM energy density, $E(\tau)$, decreases [see Fig.1(b)], but at the beginning of the era DM dominates over the DE from the point of view of energy contribution. The second era finishes with slumps of the DE energy density, of the Hubble function

and of the acceleration parameter. The DE pressure, which reached its global maximum at this moment, becomes, clearly, a locomotive power of further universe evolution. The third era can also be indicated as the era of super-acceleration, which is characterized by the growth of DE energy density and the Hubble parameter. Fourth, fifth, etc. eras can be considered in terms of relaxation to the state with asymptotically constant positive values $-q_\infty$, H_∞ , ρ_∞ and negative Π_∞ . The behavior of the DM state functions $E(\tau)$ and $P(\tau)$ during the second, third, etc. eras can not be recognized in the plots in Fig.1(b) and Fig.1(d), that is why we visualize their behavior specially in the discussion below using more appropriate scale (see Fig.11 and Fig.12).

2. Periodic models (infinite number of transition points)

We indicate the model by the term periodic when the equation $q(\tau) = 0$ has an infinite number of roots and the history of the Universe splits into infinite number of identical epochs with accelerated and decelerated expansion. Clearly, it is the case opposite to the first one (perpetually accelerated universe). Figure 2 illustrates this terminology: the DE energy density and DE pressure, as well as the Hubble function and acceleration parameter oscillate with fixed frequency and amplitude (we should keep in mind that the time scale in Fig.2 (a)-(f) is logarithmic, so that the frequency seems to be visually increasing). In the model presented in Fig.2 the DE energy density ρ is non-negative, the averaged over time (mean) value of the DE pressure $\langle \Pi \rangle$ is negative, and the sum $\rho + \Pi$ is positive. The plots in the Fig.2(e) and Fig.2(f) demonstrate that the stable oscillatory regime starts in the Universe after the second transition point. The first epoch is characterized by the decelerated expansion and consists of three eras; at the end of the first era ($\tau \simeq 10^0$) the DM contribution into the total energy density becomes negligible in comparison with the DE contribution. The second epoch relates to the accelerated expansion and can be split into two eras, the maximal value of the acceleration parameter being about 3 times smaller than for the subsequent epochs. The scale factor $a(t)$ oscillates near the de Sitter curves [see Fig.2(g)]. The periodic model can be obtained as a limiting case, when the parameter $3\xi + \sigma$ tends to its critical value $3\xi + \sigma \rightarrow 0_{+0}$.

3. Universe evolution with a finite number of transition points

Let us focus on the models for which the equation $q(\tau) = 0$ has a finite number of simple roots, $m \geq 1$. This means that during the Universe evolution the epochs with accelerated expansion are changed m times by the deceleration epochs, and vice versa. When the roots are not simple, special attention to such models is necessary, since the existence of the root does not guarantee the

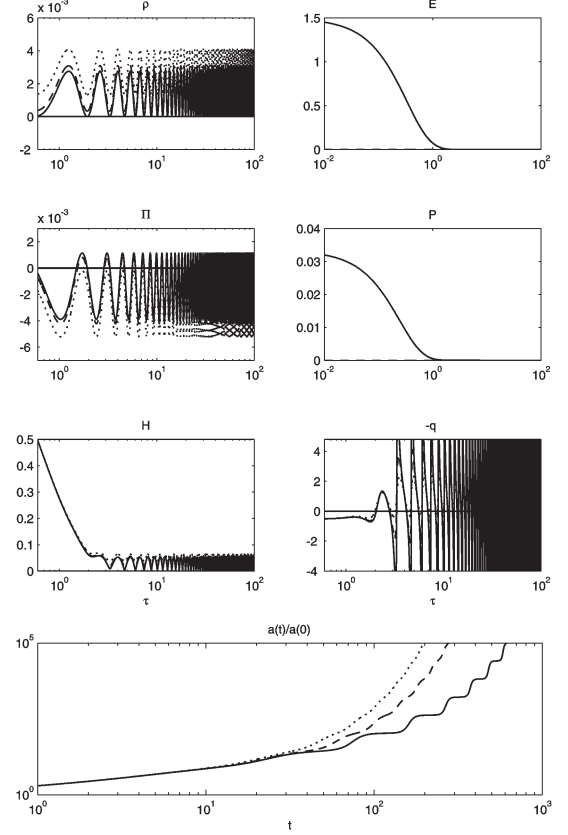


FIG. 2. Periodic universe with infinite number of acceleration/deceleration epochs. This model is a limiting case, when the parameter $3\xi + \sigma$ tends to its critical value 0_{+0} . For this model not only the sum $\rho + E$, but the DE energy density ρ itself remain non-negative. Oscillations in the plots of the Hubble function $H(\tau)$ and of the scale factor $a(t)$ are the most explicit (see dark solid line), when the parameters of the model are the following: $\xi=0.1$, $\sigma=-0.299999$ (i.e., $3\xi + \sigma \simeq 10^{-6} > 0$), $\mathcal{V}_{(0)}=1$, $E_{(0)}=0.0205$, $\lambda_{(0)}=1$, $\rho_*=0.333 \cdot 10^{-4}$, and $\Pi'(1)=0.01$.

change of the sign of the function $-q(\tau)$ (e.g., when the root is double, the curve $-q(\tau)$ touches the line $q = 0$, and this root does not give a transition point). The class of models with m transition points can be naturally divided into subclasses with $m=1$, $m=2$, etc.; every subclass can be divided into sub-subclasses according to physical and geometrical motivation. Let us focus on the basic ones.

(i) One transition point.

Figure 3 illustrates the subclass of models, for which the plot of the acceleration parameter $-q(\tau)$ (see Fig.3(f)) can be visualized as a deformed Heaviside step-function. The change of the deceleration epoch by the acceleration epoch takes place only once in a narrow time

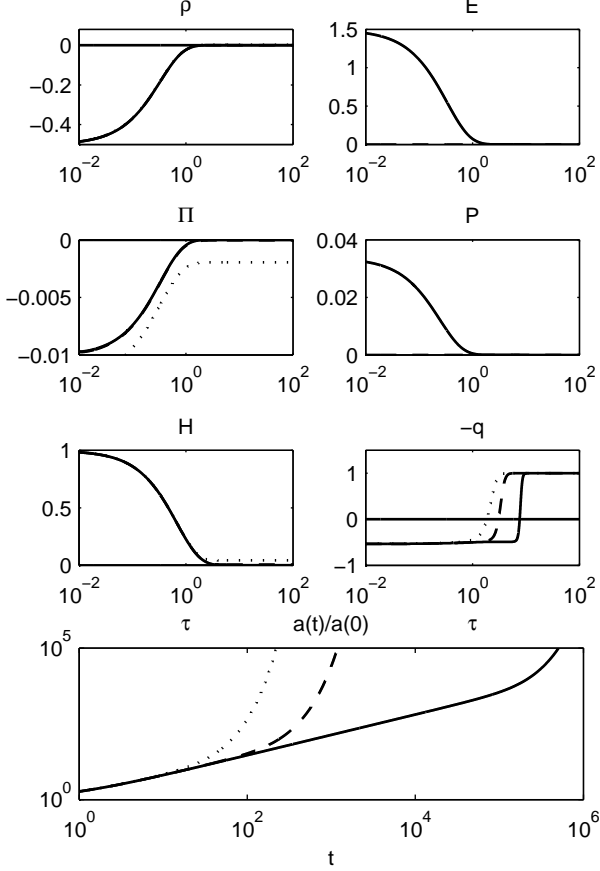


FIG. 3. The model with one transition point and $-q(\tau)$ curve of the Heaviside step-function type. The first (deceleration) epoch and the second (acceleration) epoch are not divided into eras. The epoch with the accelerated expansion is of the de Sitter-type, characterized by $\rho + \Pi = 0$. The sum $\rho(\tau) + E(\tau)$ is non-negative for arbitrary $\tau > 0$. The parameters of the model are the following: $\xi = 0.1$, $\sigma = 50$, $\mathcal{V}_{(0)} = 1$, $E_{(0)} = 0.0205$, $\lambda_{(0)} = 1$, $\rho_* = 0.333 \cdot 10^{-4}$, and $\Pi'(1) = -5$.

period, and the plot looks like a typical picture for a phase transition. Taking into account the plot of the Hubble function [see Fig.3(e)] one can conclude that the Universe's evolution starts and finishes on quasi de Sitter asymptotes with different Hubble constants $H_0 \neq H_\infty$. The functions $\rho(\tau)$, $\Pi(\tau)$, related to the DE component of the dark fluid, monotonically increase, and the functions $E(\tau)$, $P(\tau)$, related to the DM, monotonically decrease, the sum $\rho(\tau) + E(\tau)$ being non-negative for arbitrary $\tau > 0$. The second epoch, characterized by the accelerated expansion, looks like the de Sitter-type stage with $\rho + \Pi = 0$ and vanishing E and P . The first and second epochs are not divided into eras in the framework of this model.

Figure 4 illustrates an alternative subclass of models with one transition point. In contrast to the first ex-

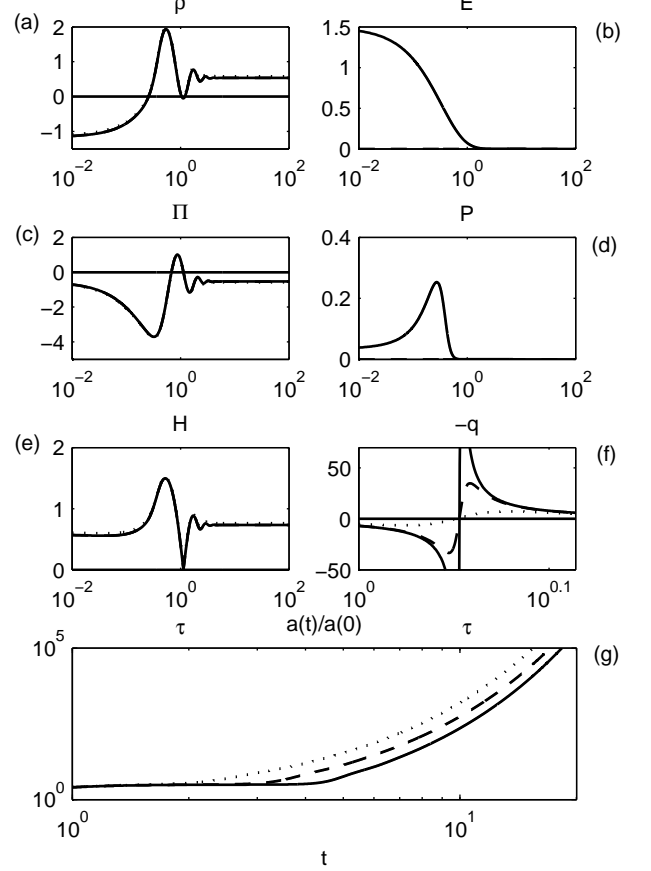


FIG. 4. The model with one transition point and two eras in both decelerated and accelerated epochs. The model describes the transition from one de Sitter-type universe to another one with different Hubble constants $H_0 \neq H_\infty$. In contrast to DM energy density, the DM pressure grows in the early universe, reaches the maximum and then decreases quickly in the deceleration epoch. The parameters of the model are the following: $\xi = 0.1$, $\sigma = 0$, $\mathcal{V}_{(0)} = 1$, $E_{(0)} = 0.0205$, $\lambda_{(0)} = 1$, $\rho_* = 0.333 \cdot 10^{-4}$, and $\Pi'(1) = -17$.

ample, the functions $\rho(\tau)$, $\Pi(\tau)$, $H(\tau)$, $P(\tau)$ and $-q(\tau)$ have extrema, so that one can pick out two eras in both epochs of the Universe history. This model also describes the transition from one de Sitter-type universe to another one with different Hubble constants $H_0 \neq H_\infty$. It is important to stress that the DM pressure $P(\tau)$ is not monotonic now: in contrast to the DM energy density, the DM pressure grows in the early Universe, reaches the maximum and then decreases quickly in the deceleration epoch.

(ii) Two transition points.

The example of the model with two transition points is given in Fig.5. The behavior of the functions $\rho(\tau)$, $\Pi(\tau)$, $E(\tau)$, and $H(\tau)$ is similar to the one, given in Fig.1, but

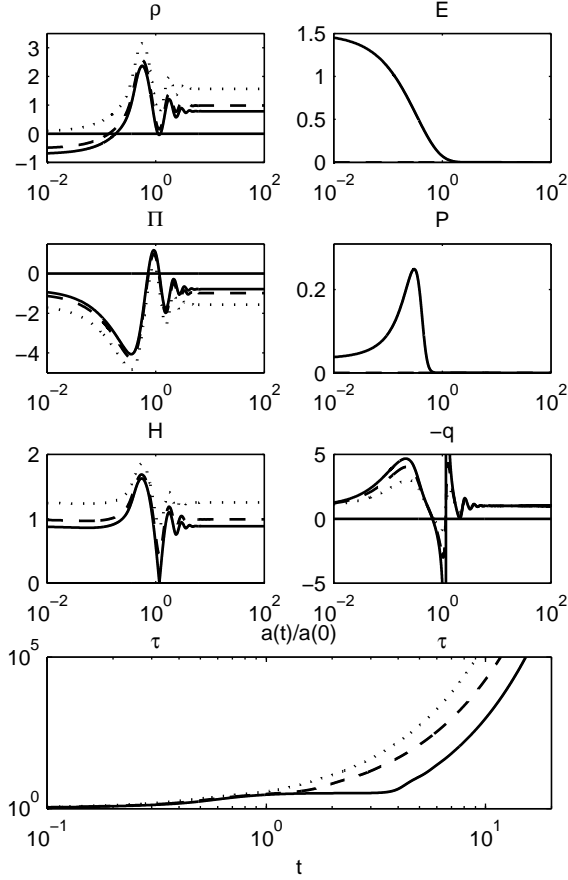


FIG. 5. The model with two transition points, two acceleration epochs and one deceleration epoch. The plots for the DE energy density, DE pressure, and Hubble functions are analogous to the curves given in Fig.1. The DM pressure has a maximum at the end of the first era of the first acceleration epoch in analogy with the curve given by Fig.4(d). The parameters of the model are the following: $\xi=0.1$, $\sigma=-0.08$, $\mathcal{V}_{(0)}=1$, $E_{(0)}=0.0205$, $\lambda_{(0)}=1$, $\rho_*=0.333 \cdot 10^{-4}$, and $\Pi'(1)=-15$.

there are new details in the panels (d) and (f). First, the DM pressure reaches maximum at the end of the first era of the first acceleration epoch. The second new detail is that the deceleration epoch appears, which separates two acceleration epochs with different asymptotic values of the Hubble function.

(iii) *Three transition points.*

The model which displays two epochs of decelerated expansion and two epochs of accelerated evolution, is presented by Fig.6. The graph of the function $-q(\tau)$ is of the so-called \mathcal{N} type. The start of the Universe's expansion relates to the deceleration epoch, which is then replaced by a short acceleration epoch as in the case of the periodic model [compare Fig.6(f) with Fig.2(f)]. The Universe's evolution during the second epoch of decel-

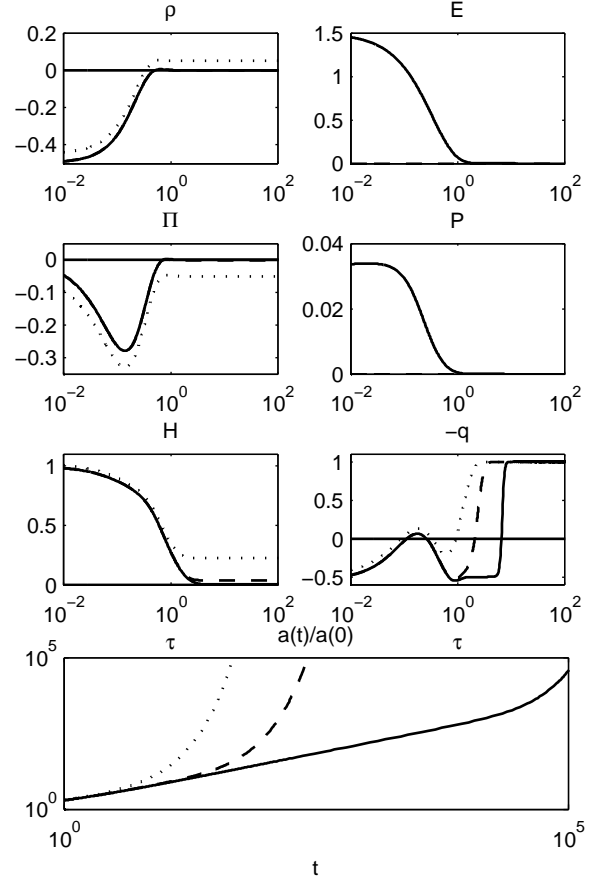


FIG. 6. The model with two epochs of decelerated expansion and two epochs of accelerated evolution. The plot of the function $-q(\tau)$ is of the so-called \mathcal{N} type. The second accelerated epoch is of the de Sitter type. The parameters of the model are the following: $\xi=0.1$, $\sigma=1$, $\mathcal{V}_{(0)}=1$, $E_{(0)}=0.0205$, $\lambda_{(0)}=1$, $\rho_*=0.333 \cdot 10^{-4}$, and $\Pi'(1)=-5$.

erated expansion and the subsequent second accelerated epoch is analogous to the model with one transition point (compare Fig.6(f) with Fig.3(f)). Clearly, the second (final) accelerated epoch is of the de Sitter type.

(iv) *Quasiperiodic evolutionary models.*

Figure 7 illustrates the behavior of the model with a big but finite number of transition points. The first, second, and third epochs of deceleration, as well as the first, second, and third epochs of accelerated expansion in this model have the same character as for the periodic model [compare with Fig.2(f)]. Nevertheless, starting from some transition point with the number (k) , i.e., when $t > t_{(\text{trans})}^{(k)}$, the curve $-q(\tau)$ remains above the line $q=0$, thus, later the Universe's expansion is accelerated. Clearly, this model is intermediate between the model with two transition points [see Fig.5] and periodic model [see Fig.2]. The behavior of the functions $\rho(\tau)$, $\Pi(\tau)$,

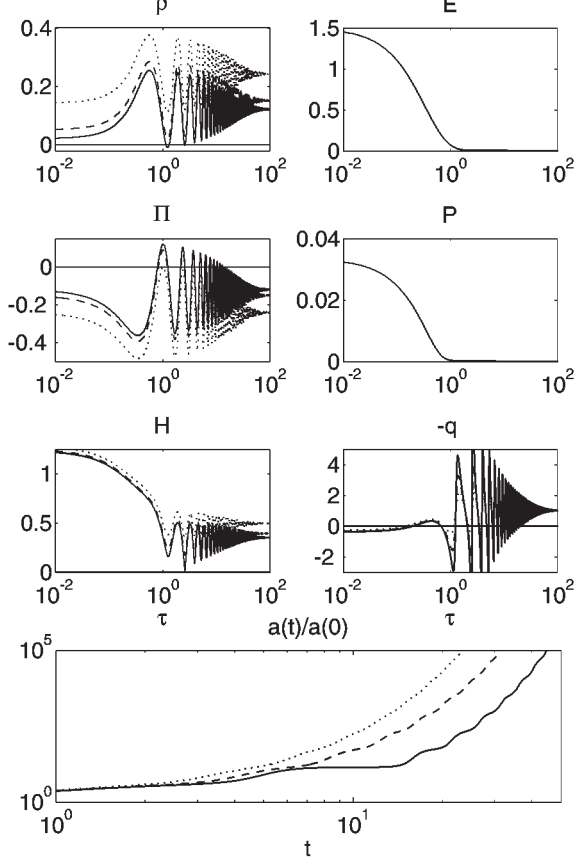


FIG. 7. The intermediate model with big but finite number of transition points. The oscillatory regime is produced by the DE component of the dark fluid, and it is switched on at the moment when the DM energy density and DM pressure become vanishing. Late-time expansion is, evidently, accelerated. The dark solid lines relate to the following parameters: $\xi=0.1$, $\sigma=-0.29$ (i.e., $3\xi+\sigma \simeq 0.01 > 0$), $\mathcal{V}_{(0)}=1$, $E_{(0)}=0.0205$, $\lambda_{(0)}=1$, $\rho_*=0.333 \cdot 10^{-4}$, and $\Pi'(1)=-1$.

$H(\tau)$ and $-q(\tau)$ is quasiperiodic: the amplitudes of their oscillations decrease asymptotically. Late-time behavior in average is of the de Sitter type with positive DE energy density and negative DE pressure. The interest in such models has been renewed after publication of the paper [35].

IV. QUALITATIVE ANALYSIS

In Sec.III we classified the solutions obtained numerically according to the number of transition points, in which the decelerated expansion of the Universe is changed by the accelerated expansion and vice versa. In order to explain the results qualitatively, below we analyze the key equations by two methods: constructing the

phase portraits and using asymptotic analysis. First of all, we consider the example of the model with $\sigma = -1$, for which the key equation can be reduced to the *autonomous* dynamic system; we find critical points and draw the corresponding phase portraits. On the basis of these results we study nonautonomous dynamic systems with $\sigma \neq -1$ taking into account that critical points of this nonautonomous system remain of the same type as for the case $\sigma=-1$, but they drift with time on the phase plane. Finally, we analyze three asymptotic limits: $\Pi \rightarrow \infty$, $\Pi \rightarrow 0$ and $\Pi \rightarrow \text{const} \neq 0$, which allow us to simplify the key equation significantly.

A. Dynamic system associated with the key equation

Let us introduce new variables $X(\tau)$, $Y(\tau)$ and τ as follows

$$X = \frac{E_* \mathcal{V}_*}{\xi(\mu+1)} x^{-\mu-1} \exp\{-\mathcal{V}_*[\Pi(x) - \Pi(1)]\},$$

$$Y \equiv \frac{\mathcal{V}_*}{(\mu+1)} x \frac{d\Pi}{dx}, \quad \tau \equiv (\mu+1) \log x. \quad (24)$$

Then the key equation of the second order (17) with the source term (19) can be rewritten as a pair of dynamic equations of the first order:

$$\frac{dX}{d\tau} = -X(1+Y),$$

$$\frac{dY}{d\tau} = -A + Y(X-B) + \frac{3(1+\sigma)}{\xi(\mu+1)^2} \left[\tau + \log \left(\frac{\xi(\mu+1)}{E_* \mathcal{V}_*} X \right) \right], \quad (25)$$

where

$$A \equiv \frac{3\rho_0^* \mathcal{V}_*}{\xi(\mu+1)^2}, \quad B \equiv \frac{3\xi + \sigma}{\xi(\mu+1)}. \quad (26)$$

The quantity $X(\tau)$ is non-negative due to its definition (24). X tends to zero in two different cases: first, when $\Pi \rightarrow \infty$, or second, asymptotically at $x \rightarrow \infty$, if $\Pi(\infty)$ is finite. The initial value for the parameter τ , $\tau=0$ relates to the moment $t=t_0$ and, respectively, $x=1$, then initial data for the integral curves in terms of these variables are the following:

$$X(0) = \frac{E_* \mathcal{V}_*}{\xi(\mu+1)}, \quad Y(0) = \frac{\mathcal{V}_*}{(\mu+1)} \Pi'(1). \quad (27)$$

Generally, this dynamic system is nonautonomous because of the term linear in τ in the second equation. Nevertheless, there is a case $\sigma=-1$ when the system (25) becomes autonomous. Let us consider this case in more detail.

1. Autonomous dynamic system at $\sigma = -1$

The autonomous dynamic system

$$\frac{dX}{d\tau} = -X[1+Y], \quad \frac{dY}{d\tau} = -A + Y[X-B] \quad (28)$$

contains only two control parameters: A and B , the parameter A being now positive. The new dimensionless parameter

$$\theta \equiv \frac{B}{A} = \frac{(3\xi - 1)(\mu + 1)}{3\rho_0\mathcal{V}_*} \quad (29)$$

plays an interesting role in further analysis. Physically appropriate integral curves should be situated in the domain $X \geq 0$ on the plane XOY . We consider the integral curves, which penetrate into the domain $X < 0$, as non-admissible and omit the models with the corresponding set of guiding parameters. The qualitative analysis of the two-parameter autonomous dynamic system (28) demonstrates the following interesting features.

2. Critical points

When $A \neq B$ and $B \neq 0$, there are two critical points associated with this dynamic system. The first critical point

$$X_{(1)} = 0, \quad Y_{(1)} = -\frac{A}{B} = -\frac{1}{\theta} \quad (30)$$

is the saddle one, when $\theta < 1$, and is the stable nodal point, when $\theta > 1$. The second critical point is

$$X_{(2)} = B - A = (\theta - 1)\frac{3\rho_0\mathcal{V}_*}{\xi(\mu + 1)^2}, \quad Y_{(2)} = -1, \quad (31)$$

and it coincides with the first one, when $B=A$, i.e., when $\theta=1$. Generally, the second critical point can be

- (i) the saddle point, when $\theta > 1$ (the first critical point is the nodal one);
- (ii) the stable nodal point, when $\frac{3\rho_0\mathcal{V}_*}{4\xi(\mu+1)^2} > 1-\theta > 0$ (the first critical point is the saddle one);
- (iii) the stable focus, when $0 < \frac{3\rho_0\mathcal{V}_*}{4\xi(\mu+1)^2} < 1-\theta$ (the first critical point is the saddle one); or
- (iv) the degenerated node, when $0 < \frac{3\rho_0\mathcal{V}_*}{4\xi(\mu+1)^2} = 1-\theta$ (the first critical point is the saddle one).

3. Two phase portraits of the autonomous dynamic system

A typical phase portrait of the autonomous dynamic system with a stable node and a saddle point is presented in Fig.8. Integral curves in the northern and western domains, which are cut out by the separatrices of the saddle point with coordinates $X_{(2)}=0.2125, Y_{(2)}=-1$, tend asymptotically to the nodal point with $X_{(1)}=0$,

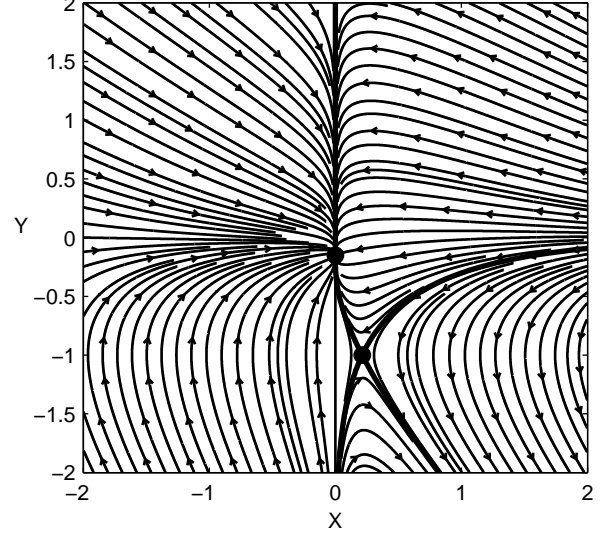


FIG. 8. Phase portrait of the autonomous dynamic system with stable node at $X_{(1)}=0, Y_{(1)}=-0.15$ and saddle point at $X_{(2)}=0.2125, Y_{(2)}=-1$. Integral curves in the northern and western domains, which are cut out by the separatrices of the saddle point, tend asymptotically to the node. Integral curves in the southern and eastern domains of this saddle point can be asymptotically characterized by infinite values of X and/or Y .

$Y_{(1)}=-0.15$. All the integral curves in the southern and eastern domains of this saddle point can be asymptotically characterized by infinite values of X and/or Y .

A typical phase portrait of the autonomous dynamic system with a focus and a saddle point is given in Fig.9. The domain of quasiperiodic motion is situated in the south-western domain, which is cut out by the separatrices of the saddle point at $X_{(1)}=0, Y_{(1)}=0.25$. This quasiperiodic motion is associated with the presence of the focus at $X_{(2)} = -0.59375, Y_{(2)} = -1$. Curves walking in three other domains are asymptotically unstable.

B. On the behavior of the nonautonomous dynamic system with $\sigma > -1$

When $\sigma=-1$ and the dynamic system is autonomous, there are two typical phase portraits, given by Fig.8 and Fig.9. The qualitative difference between them is predetermined by specific combinations of the guiding parameters ξ, ρ_0 , and \mathcal{V}_* : any changes on the phase space are associated with variations of these guiding parameters. Typical phase portraits with fixed guiding parameters remain unchanged with time, and the integral curves can be prolonged till $\tau \rightarrow \infty$. When $\sigma > -1$, the dynamic system is nonautonomous, nevertheless, one can describe such a model qualitatively in terms of instantaneous phase portrait distortion, in terms of (quasi)critical points drift, and their transformations. One can stress

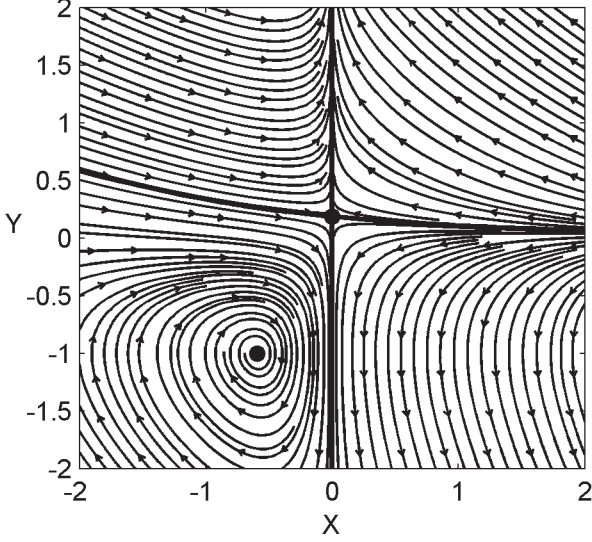


FIG. 9. Phase portrait of the autonomous dynamic system with stable focus and saddle point. The domain of quasiperiodic motion is situated in the south western domain, which is cut out by the separatrices of the saddle point at $X_{(1)}=0$, $Y_{(1)}=0.1875$. The focus is situated at $X_{(2)}=-0.59375$, $Y_{(2)}=-1$.

that in this case a restructuring of the instantaneous phase portraits can take place because of time growth, when the guiding parameters remain unchanged.

1. Critical points drift and transformation

Let us consider a close vicinity of the point $\tau=\tau_0$ and put the value τ_0 to the right-hand side of the second equation (25). In the small vicinity of τ_0 ($\tau=\tau_0+\eta$, and $\eta \ll \tau_0$ is a small deviation) we can consider (quasi) critical points in analogy with true critical points, studied in the previous case. The first (quasi) critical point relates to $X_{(1)}=0$, $Y_{(1)}=\infty$, when $3\xi+\sigma < 0$, and $X_{(1)}=0$, $Y_{(1)}=-\infty$, when $3\xi+\sigma > 0$. In both cases these points disappear from the admissible part of the dynamic plane XOY . Other (quasi) critical points relate to the value $Y_{(2)}=-1$, and the corresponding values X can be found from the transcendent equation

$$X - \beta \log X = \mathcal{K}(\tau_0), \quad \beta \equiv \frac{3(1+\sigma)}{\xi(\mu+1)^2} \geq 0, \quad (32)$$

$$\mathcal{K}(\tau_0) = \beta \left[\tau_0 + \log \frac{\xi(\mu+1)}{E_* \mathcal{V}_*} + \frac{(3\xi+\sigma)(\mu+1) - 3\rho_0^* \mathcal{V}_*}{3(1+\sigma)} \right]. \quad (33)$$

The plot of the function $f(X) \equiv X - \beta \log X$ is presented in Fig.10. The function $f(X)$ has the minimum $f_{(\min)} = \beta \log \frac{e}{\beta}$ at $X=\beta$, which divides the corresponding curve into two branches: the first of them is situated at

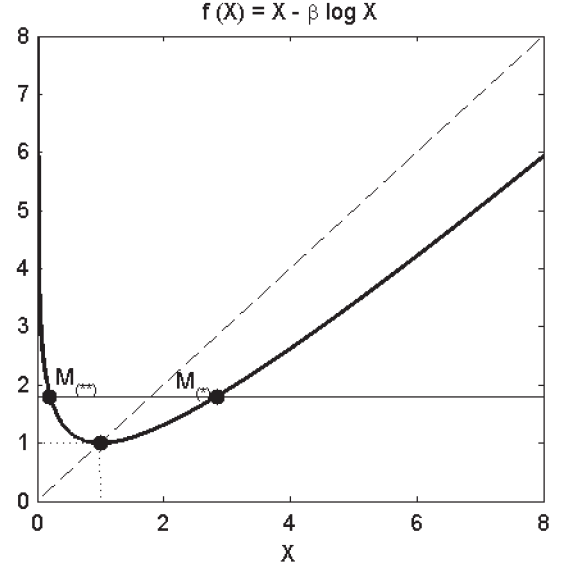


FIG. 10. The plot illustrates the appearance of a pair of (quasi)critical points, when the cosmological time increases. The function $f(X) \equiv X - \beta \log X$ has the minimum $f_{(\min)} = \beta \log \frac{e}{\beta}$ at $X=\beta$; the point of minimum divides the plot of this function into two branches: first of them is situated at $0 < X < \beta$, the second one relates to the interval $X > \beta$. Clearly, Eq. (32) has no solutions, when $\mathcal{K}(\tau_0) < \beta \log \frac{e}{\beta}$; it has only one (double) root, when $\mathcal{K}(\tau_0) = \beta \log \frac{e}{\beta}$; there are two different roots, when $\mathcal{K}(\tau_0) > \beta \log \frac{e}{\beta}$, the corresponding points indicated as $M_{(*)}$ and $M_{(**)}$. The curve on the plot corresponds to the value $\beta = 1$.

$0 < X < \beta$ (left branch), and the second one relates to the interval $X > \beta$ (right branch). Clearly, Eq. (32) has no solutions, when $\mathcal{K}(\tau_0) < \beta \log \frac{e}{\beta}$ or equivalently when $\tau_0 < \tau_{(\text{crit})}$, where the critical time moment is

$$\tau_{(\text{crit})} = 1 + \frac{\rho_0^* \mathcal{V}_*}{1+\sigma} - \frac{(\mu+1)(3\xi+\sigma)}{3(1+\sigma)} + \log \frac{(\mu+1)\mathcal{V}_* E_*}{3(1+\sigma)}. \quad (34)$$

Eq. (32) has only one (double) root, when $\mathcal{K}(\tau_0) = \beta \log \frac{e}{\beta}$, or $\tau_0 = \tau_{(\text{crit})}$; there are two different roots, when $\mathcal{K}(\tau_0) > \beta \log \frac{e}{\beta}$ or equivalently $\tau_0 > \tau_{(\text{crit})}$. In other words, there are no (quasi)critical points at $\tau_0 < \tau_{(\text{crit})}$, one point appears at $\tau_0 = \tau_{(\text{crit})}$, and two (quasi)critical points appear in the instantaneous phase portrait, when $\tau_0 > \tau_{(\text{crit})}$.

The first (quasi)critical point indicated as $M_{(*)}(\tau_0)$ drifts to infinity, since the value $X_{(*)}$, for which the right branch of the curve happens to be crossed by the horizontal straight line, increases with τ_0 . In order to recognize the type of this (quasi) critical point, let us find the roots of the characteristic equation associated with the dynamic system in the vicinity of the point with coordinates $(X_{(*)}, -1)$,

$$\lambda_{1,2} = \frac{1}{2} \left[X_{(*)} - B \pm \sqrt{(X_{(*)} - B)^2 + 4(X_{(*)} - \beta)} \right]. \quad (35)$$

At the critical moment of time the equality $X_{(*)} = \beta$ takes place, and we deal with the degenerated node; when

$X_{(*)} > \beta$, there are two real roots of different signs, thus the (quasi)critical point is the saddle one.

The second (quasi)critical point $M_{(**)}$ drifts to the point $(0, -1)$ when τ_0 increases, since the value $X_{(**)} \leq \beta$, for which the left branch of the curve crosses the horizontal straight line, tends to zero. The type of the second (quasi)critical point depends on the value τ_0 and on the relation between parameters B and β .

(i) When $B > 1 + \beta$, or equivalently

$$\sigma > \frac{3}{\mu-2} + \xi(\mu+1), \quad (36)$$

the discriminant in (35) is always positive, the roots of characteristic equations are real and negative, thus the second (quasi)critical point is a stable node for each $\tau_0 > \tau_{(\text{crit})}$. We deal with the phase portrait, which contains a stable node $M_{(**)}$ and a saddle point $M_{(*)}$.

(ii) When $B < 1 + \beta$ we face the reconstruction of the phase portraits with time. Indeed, one can fix two moments of time, $\tau_0^{(1)}$ and $\tau_0^{(2)}$, defined as

$$X_{(**)}(\tau_0^{(1)}) \equiv B - 2 + 2\sqrt{1 + \beta - B},$$

$$X_{(*)}(\tau_0^{(2)}) \equiv B - 2 - 2\sqrt{1 + \beta - B}, \quad (37)$$

for which the discriminant in (35) takes zero value. Since $X_{(**)}$ tends to zero with time, one obtains three subsequent situations: first, when $\tau_{(\text{crit})} < \tau_0 < \tau_0^{(1)}$ the roots are real, i.e., $M_{(**)}$ is a node; second, when $\tau_0^{(1)} < \tau_0 < \tau_0^{(2)}$, the roots are complex numbers, i.e., $M_{(**)}$ is a focus; third, when $\tau_0^{(2)} < \tau_0$ the roots are real again, i.e., $M_{(**)}$ is a node. One can guarantee, that the nodes and focus are stable, if $\beta < B < 1 + \beta$.

(iii) If $B < \beta$, evidently, there exists a moment $\tau_0^{(3)}$, when the decreasing quantity $X_{(**)}(\tau_0) < \beta$ becomes equal to the parameter B . At this moment $\lambda_{1,2} = \pm i\sqrt{\beta - B}$, i.e., the focus transforms into a center. It is possible, when

$$-1 < \sigma < 3 \frac{[1 - \xi(\mu+1)]}{(\mu-2)}, \quad \xi < \frac{1}{3}. \quad (38)$$

Finally, at the moments $\tau_0^{(1)}$ and $\tau_0^{(2)}$ the discriminant in (35) vanishes, i.e., the corresponding points should be classified as degenerated nodes.

2. Phase portrait distortion and transformation

Let us consider the plots in Fig.1(c),2(c),3(c),4(c),5(c),6(c), and 7(c), obtained numerically, from the point of view of *qualitative* analysis of the models with $\sigma > -1$. In fact we take two typical phase portraits: for a node and a saddle point [Fig.8], and for a focus and saddle point [Fig.9], and provide the changes of two types. First, we move the

(quasi)critical points horizontally, thus distorting the instantaneous phase portrait; second, we replace the node by focus and vice-versa, thus modeling transitions in the instantaneous phase portraits with time.

1. Figure1(c): *perpetually accelerated universe*.

For the given values of the guiding parameters we have $\sigma < 3 + 4\xi$, i.e., the inequality $B < 1 + \beta$ is valid [see the discussion of Eq. (37) above]. The zone $\tau < 10^0$ can be indicated as precritical, the function $\Pi(\tau)$, the DE pressure, decreases there, since the initial value $\Pi'(1) = -1$ is negative. Then, as it was qualitatively predicted, the focus appears on the instantaneous phase portrait, so that the DE pressure enters the zone of damped quasioscillations.

2. Figure 2(c): *periodic universe*.

For this model, clearly, both inequalities given by (38) are valid; in addition $B < 1 + \beta$, thus it is a typical model with center [see the discussion of Eq. (38) above]. The presence of a center on the phase portrait explains the periodic graph of the DE pressure $\Pi(\tau)$ (the graph is presented in a logarithmic scale).

3. Figure 3(c): *first model with one transition point*.

There, clearly, the inequality (36) is valid, i.e., $B > 1 + \beta$ and we deal with the absence of focuses. Instantaneous phase portraits contain stable nodes only, the graph for the DE pressure has no quasioscillations.

4. Figure 4(c): *second model with one transition point*.

5. Figure 5(c): *model with two transition points*.

There, in both cases, we deal with the situation similar to the one in Fig.1(c).

6. Figure 6(c): *model with three transition points*.

The situation is analogous to the case given by Fig.3(c).

7. Figure 7(c): *quasiperiodic universe*. Again we deal with the set of guiding parameters, for which $B < 1 + \beta$, and thus the stable focus appears in the instantaneous phase portrait of the dynamic system; quasioscillations of the DE pressure are typical for this model.

C. Asymptotic behavior of the integral curves

Speaking about nonrelativistic and ultrarelativistic models, we distinguish between *initially* and *effectively* hot or cold states of the DM particles. When the parameters $\lambda_{(a)} \equiv \frac{m_{(a)} c^2}{k_{(B)} T_{(a)}}$ are much bigger or much smaller than 1, we deal with initially nonrelativistic or ultrarelativistic DM, respectively. In the course of the Universe expansion an initially cold DM can become effectively hot (effectively ultrarelativistic), when the term $F_{(a)}(x) \rightarrow \infty$ [see (14)]. Such terminology is advocated by the fact, that at $F_{(a)}(x) \rightarrow \infty$ one obtains $\langle q^2 \rangle > F_{(a)}(x) \gg 1$, and the averaged kinetic energy of a DM particle becomes much bigger than the corresponding rest energy, even if initially at $t=t_0$ ($F(1)=1$) the inequality had the form $\langle q^2 \rangle < 1$. Analogously, when $F_{(a)}(x) \rightarrow 0$, an initially hot DM converts into the effectively nonrelativistic, because the rest energy dominates over the kinetic energy of a DM particle. A new interesting case

can appear due to the Archimedean-type force, when $F_{(a)}(x) \rightarrow \text{const} \neq 0$, despite the fact that $a(t) \rightarrow \infty$. In this case one deals with the asymptotic fixation of the degree of relativism of the DM particles instead of standard effective cooling. Let us consider these asymptotic cases and analyze the model behavior for arbitrary values of the parameters $\lambda_{(a)}$.

1. Asymptotic regime $F_{(a)}(x) \rightarrow \infty$

In the absence of the Archimedean-type force, i.e., at $\mathcal{V}_{(a)} = 0$, the function $F_{(a)}(x) = x^{-2}$ tends to zero asymptotically. When $\mathcal{V}_{(a)} \neq 0$, the function $F_{(a)}(x)$ can tend to infinity if the DE pressure takes negative infinite value, $\Pi(x) \rightarrow -\infty$. In this asymptotic regime, when $F_{(a)}(x) \rightarrow \infty$, the integrals in (12), (13), (18) can be easily calculated yielding

$$\mathcal{J}(x) = \frac{\Pi'(x)}{x^3} \sum_{(a)} E_{(a)} \mathcal{V}_{(a)} I_{(a)} e^{\mathcal{V}_{(a)}[\Pi(1) - \Pi(x)]}, \quad (39)$$

$$E(x) = 3P(x) = \frac{1}{x^3} \sum_{(a)} E_{(a)} I_{(a)} e^{\mathcal{V}_{(a)}[\Pi(1) - \Pi(x)]}, \quad (40)$$

where the parameter $I_{(a)}$ is given by

$$I_{(a)} \equiv 2\lambda_{(a)}^{-4} [\lambda_{(a)}^2 + 3\lambda_{(a)} + 3] e^{-\lambda_{(a)}}. \quad (41)$$

Let us indicate the maximal parameter from the set $\{\mathcal{V}_{(a)}\}$ as ν , the corresponding parameter $E_{(a)}$ as E and $I_{(a)}$ as I . Then one obtains that, when $\sigma > -1$ and $x \rightarrow \infty$, the leading order term in the left-hand side of the key equation (17) is $3(1+\sigma)\Pi$ and the reduced equation for $\Pi(x)$ is of the form

$$\Pi'(x) = \frac{3(1+\sigma)}{\nu EI} x^3 \Pi(x) \exp\{\nu \Pi(x)\}. \quad (42)$$

This means that at $\Pi \rightarrow -\infty$ the derivatives Π' , Π'' , etc., asymptotically vanish, and the behavior of the DE pressure $\Pi(x)$ is described by the function inverse to the integral exponent $Ei^{-1}(\Pi)$, where $Ei(\Pi) = \int \frac{d\Pi}{\Pi} e^{-\nu \Pi}$. The decomposition of this function at $\Pi \rightarrow -\infty$ gives the transcendent equation

$$\frac{1}{\Pi} \exp\{-\nu \Pi(x)\} = -\frac{3(1+\sigma)}{4EI} x^4. \quad (43)$$

When $\sigma = -1$, the asymptotic law is $\Pi(x) \rightarrow -\frac{4}{\nu} \log x$ in accordance with the exact solution of the anti-Gaussian type, studied in the first part of the work [13]. The asymptotic behavior of the DE energy density is given by the formula $\rho(x) \simeq \sigma \Pi$ [see (11)] and depends essentially on the sign of the parameter σ : it remains positive at $\Pi(x) \rightarrow -\infty$, when $-1 < \sigma < 0$. Concerning the DM energy density $E(x)$ and DE pressure $P(x)$, these quantities grow exponentially; we do not consider the Hubble function $H(x)$ and the scale factor $a(t)$ for such models, since there is no observational data, which could confirm such behavior.

2. Asymptotic regime $F_{(a)}(x) \rightarrow 0$

This asymptotic regime can be realized, when the DE pressure takes arbitrary positive or finite negative value at $x \rightarrow \infty$. The asymptotic behavior of this type relates to the vanishing source term

$$\mathcal{J}(x) \rightarrow \frac{3\Pi'}{x^4} \mathcal{N} \exp\{2\mathcal{V}_{(a)}[\Pi(1) - \Pi(x)]\},$$

$$\mathcal{N} = \sum_{(a)} N_{(a)} k_{(B)} T_{(a)} \mathcal{V}_{(a)} \frac{K_3(\lambda_{(a)})}{K_2(\lambda_{(a)})}, \quad (44)$$

and vanishing DM energy density

$$E(x) = \frac{1}{x^3} \sum_{(a)} N_{(a)} m_{(a)}. \quad (45)$$

Thus, the DE pressure satisfies now the Euler equation

$$\xi x^2 \Pi''(x) + x \Pi'(x) (4\xi + \sigma) + 3(1+\sigma)\Pi + 3\rho_0 = 0, \quad (46)$$

which is studied in detail in Sec.III A of the first part of our work [13]. In particular, in Sec.III A 3, we have shown that there exist quasiperiodic oscillations near the asymptote $\Pi(x) = -\frac{\rho_0}{1+\sigma}$, which are manifestly presented in Fig.1(c), Fig.4(c), Fig.5(c), Fig.7(c). The aperiodic solutions studied in Sec.III A 1, and Sec.III A 2 [13] clearly appear in Figs.3(c) and 6(c).

3. Asymptotic regime $F_{(a)}(x) \rightarrow \text{const} \neq 0$

Let us suppose for simplicity that $\mathcal{V}_{(a)} = \nu$ for all types of the DM particles, and let the corresponding function $F(x)$ tend to a nonvanishing constant value F_∞ , when $x \rightarrow \infty$. This means that asymptotic behavior of the DE pressure is the following

$$\Pi(x) \rightarrow \Pi(1) - \frac{1}{\nu} \log x - \frac{1}{2\nu} \log F_\infty. \quad (47)$$

Then the initial data require that $F_\infty = 1$, and the source term (18) takes asymptotically the following form

$$\mathcal{J}(x) \rightarrow -\frac{3\nu}{x^3} \sum_{(a)} N_{(a)} k_{(B)} T_{(a)}, \quad (48)$$

i.e., it decreases as x^{-3} at $x \rightarrow \infty$. The left-hand side of Eq. (17) vanishes after the substitution of (47), if $\sigma = -1$ and $3\rho_0\nu = 3\xi - 1$, i.e., the asymptotic regime exists at special conditions only. The DE and DM energy densities behave in this case as

$$\rho(x) \rightarrow \frac{1}{\nu} \log x,$$

$$E(x) \rightarrow \frac{1}{x^3} \sum_{(a)} N_{(a)} k_{(B)} T_{(a)} \left[\lambda_{(a)} \frac{K_3(\lambda_{(a)})}{K_2(\lambda_{(a)})} - 1 \right]. \quad (49)$$

The Hubble function, scale factor and acceleration parameters are given by the following formulas

$$H(x) \rightarrow \sqrt{\frac{8\pi G}{3\nu} \log x}, \quad a(t) \rightarrow a(t_0) \exp \left\{ \frac{2\pi G}{3\nu} t^2 \right\},$$

$$-q(t) \rightarrow 1 + \frac{3\nu}{4\pi G t^2}, \quad (50)$$

which, clearly, describe the anti-Gaussian solution studied in the first part of the work [13].

V. DISCUSSION

The Archimedean-type model can describe qualitatively two cornerstones of the Universe's evolution: the inflation in the early Universe and the late-time accelerated expansion. Also, this model offers a variant explanation of the so-called coincidence problem, and it gives some motivation for the specific division of the Universe's history into epochs and eras. Let us consider these questions in more detail.

A. Inflation in the early Universe

When $\tau \leq 1$ Fig.1(a), 2(a), 3(a), 4(a), 5(a), 6(a), and 7(a) display the first inflationary-type epoch: one can reveal a quick growth of the DE energy density $\rho(\tau)$. During this period of the Universe evolution the scale factor $a(t)$ increases essentially: in order to visualize this inflationary effect we presented additionally the fragment of the plot $a(t)$ in the natural scale t instead of the logarithmic one [see Fig.11(a)]. The steepness of the plot of $a(t)$ is predetermined by the combination of the guiding parameters; there are a lot of possibilities to fit the observed curve by the curve predicted in the framework of the Archimedean-type model. In the context of expansion the growth of the DE energy density $\rho(\tau)$ in the early Universe relates to the heating of the DE component of the dark fluid. Clearly [compare, e.g., the panels (a) and (b) in Figs.1-7] the sum $\rho + E$ remains non-negative for the whole interval of time. This feature provides the H^2 to be non-negative, which guarantees that H is a real function. At the same time the DM energy density $E(\tau)$ [see the panels (b)] decreases monotonically; nevertheless, the rate of its effective cooling differs essentially from the rate given by the standard powerlaw function ($1/a^4$ for the ultrarelativistic DM or $1/a^3$ for the cold DM). Principally new detail can be found in Fig.4(d) and Fig.5(d): the DM pressure is described by a nonmonotonic function; it grows quickly, reaches a maximum, and then decreases rapidly.

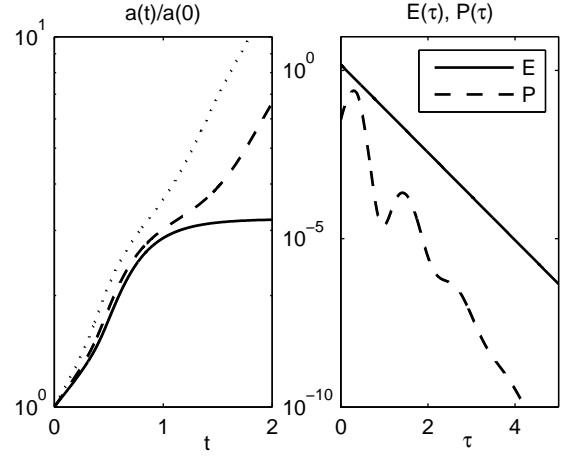


FIG. 11. In the left panel a fragment of the plot is presented, which illustrates the inflationary-type growth of the scale factor $a(t)$ for the early Universe, given in terms of cosmological time t . In the right panel one can see a typical late-time behavior of $E(\tau)$ and $P(\tau)$; this rescaled fragment illustrates the features of the DM evolution at $\tau > 1$, which cannot be recognized on the plots given by Fig.1(b,d)-Fig.7(b,d).

B. Late-time accelerated expansion

When $\tau \rightarrow \infty$, the curves $-q(\tau)$, which present the evolution of the acceleration parameter in Fig.1(f), 2(f), 3(f), 4(f), 5(f), 6(f), and 7(f) tend to the horizontal asymptote, the value $-q(\infty)$ being positive. Taking into account the behavior of the plots of the Hubble functions displayed in Fig.1(e), Fig.3(e)-Fig.7(e), one can conclude that $H(\tau \rightarrow \infty) \rightarrow H_\infty$, i.e., the Hubble function also tends to the positive constant value, when $\tau \rightarrow \infty$. This means, first, that a typical behavior of the Universe with Archimedean-type interaction between DE and DM is characterized by the late-time accelerated expansion; second, that asymptotically the Archimedean-type model converts into the quasi-de Sitter one.

The DM state functions $E(\tau)$ and $P(\tau)$ decrease rapidly, and for $\tau > 1$ we should change the scale in order to visualize the behavior of these functions. A typical late-time behavior of $E(\tau)$ and $P(\tau)$ is presented in the right panel of Fig.11. In order to describe the effective equation of state of dark matter in the framework of the Archimedean-type model, we calculated numerically the ratio $w(\tau) \equiv \frac{P(\tau)}{E(\tau)}$; the plot of the function $w(\tau)$ is presented in the left panel of Fig.12. Clearly, this function is constrained: $0 < w(\tau) < 1$; maximal value of this ratio is about $1/3$ in the first epoch of the Universe's evolution, when the DM can be considered as an effectively ultrarelativistic substrate. In the early Universe the DM state evolves quasiperiodically, i.e., the eras with effective cooling were changed by the eras of effective heating. Starting from $\tau \simeq 4$ the function $w(\tau)$ tends to zero linearly in $\tau = \log \frac{a(t)}{a(t_0)}$, i.e., the DM behaves effectively

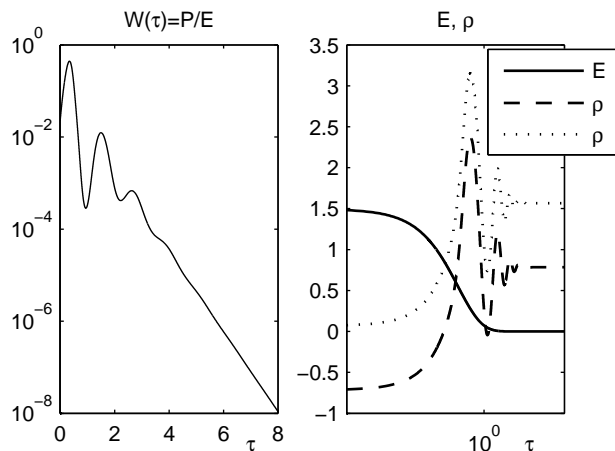


FIG. 12. The left panel contains the plot of the ratio $w(\tau) = \frac{P(\tau)}{E(\tau)}$, which presents the effective equation of state for the DM component of the dark fluid. Maximal value of this ratio is about 1/3 in the first epoch of the Universe's evolution, when the DM can be considered as an effectively ultrarelativistic substrate. In the early Universe the DM state evolves quasiperiodically; starting from $\tau \simeq 4$ the function $w(\tau)$ tends to zero linearly in τ , i.e., the DM behaves effectively as a cold gas (dust). The right panel displays the cross-points of the ρ and E plots. This example illustrates the so-called coincidence problem: why the energy densities of the DE and DM components of the dark fluid are of the same order today (72% and 23%, respectively).

as a cold gas (dust).

C. Coincidence problem

Although the DE and DM components of the dark fluid evolve at different rates throughout the history of the Universe, their magnitudes are of the same order today (72% and 23%, respectively). This is known as the coincidence problem [36]–[39]. The Archimedean-type model could help us to make a step toward solving this problem. In the right panel of Fig.12 we placed the example of the plots describing the DE and DM evolution with time τ . The guiding parameter ρ_0^* defines the asymptotical ratio between ρ and E ; this ratio can in principle be chosen so that $\frac{\rho}{E} \rightarrow \frac{72}{23}$. Other guiding parameters define how many cross-points of the ρ and E plots can exist. For instance, in Fig.12 there are examples with one and three cross-points. Using the guiding parameters we can remove one of the cross-points away from the point $\tau \simeq 1$, but we hope to discuss in detail the fitting problem in a special work.

D. On the partition of the Universe's history into epochs and eras and its multi-inflationary behavior

There are a few versions of dividing the history of the Universe into self-sufficient parts that are interest-

ing from a physical point of view. For instance, one can consider the Hubble function $H(t)$, find its zeros and extrema and separate the admissible time interval in line with them (see, e.g., [40]). We attached such a partition to the function $-q(t)$, i.e., based the classification of models on the zeros and extrema of the acceleration parameter. This seems to be motivated, since we are interested in picking out the epochs of accelerated and decelerated expansion of the Universe, thus the transition points appeared as points, in which the function $-q(t)$ changes the sign. We have shown above that there are a lot of models in which the Universe's history is multistage. In particular, the Universe's evolution can be quasiperiodic, and one can use the term *multi-inflationary* evolution, the first inflation being the sharpest, others being more and more smoothed. Following this line, we divide the epochs into eras by using the maximums and minimums of this function: this is equivalent to the method of statefinders proposed in [34]. We hope to consider such fine details of the Universe's history partition in a special work.

E. Conclusions

The model of Archimedean-type coupling between dark energy and dark matter makes it possible to explain the principal cornerstones of the Universe's evolution: the early-time inflationary expansion, the late-time accelerated expansion, and the coincidence phenomenon.

The model of Archimedean-type coupling between dark energy and dark matter possesses a wide set of guiding parameters suitable for fitting of the model predictions to the observational data; we hope to devote a special work to this important question.

The model of Archimedean-type coupling offers a natural approach to the partition of the Universe's history into epochs and eras using the number of transition points and number of extrema of the function $-q(t)$, the acceleration parameter of the Universe's evolution. The model allows us to speak about multistage evolution and about the multi-inflationary behavior of the Universe.

VI. ACKNOWLEDGMENTS

The authors are grateful to Professor W. Zimdahl for fruitful discussions, comments and advice. This work was partially supported by the Russian Foundation for Basic Research (Grants No. 08-02-00325-a and 09-05-99015) and by Federal Targeted Programme, Scientific and Scientific-Pedagogical Personnel of the Innovative Russia (Grants No. 16.740.11.0185 and 14.740.11.0407).

-
- [1] E.J. Copeland, M. Sami and S. Tsujikawa, *Int. J. Mod. Phys. D* **15**, 1753 (2006).
 - [2] J. Frieman, M. Turner and D. Huterer, *Ann. Rev. Astron. Astrophys.* **46**, 385 (2008).
 - [3] T. Padmanabhan, *Gen. Relat. Grav.* **40**, 529 (2007).
 - [4] A. Del Popolo, *Astronomy Reports*, **51**, 169 (2007).
 - [5] G. Lazarides, *Lect. Notes Phys.* **720**, 3 (2007).
 - [6] J. Silk, *Lect. Notes Phys.* **720**, 101 (2007).
 - [7] J. Ren and Xin-He Meng, *Int. J. Mod. Phys. D* **16**, 1341 (2007).
 - [8] S. Nojiri and S.D. Odintsov, *Phys. Lett. B* **649**, 440 (2007).
 - [9] I. Brevik, E. Elizalde, O. Gorbunova and A. V. Timoshkin, *Eur. Phys. J. C* **52**, 223 (2007).
 - [10] A. Arbey, *Open Astronomy Journal*, **1**, 27 (2008).
 - [11] S. Nojiri and S.D. Odintsov, Unified cosmic history in modified gravity: from F(R) theory to Lorentz non-invariant models (arXiv:1011.0544).
 - [12] W.S. Hipolito-Ricaldi, H.E.S. Velten and W. Zimdahl, arXiv:0902.4710.
 - [13] A.B. Balakin and V.V. Bochkarev, *Phys. Rev. D* **83**, 024035 (2011).
 - [14] W. Zimdahl and A.B. Balakin, *Phys. Rev. D* **58**, 063503 (1998).
 - [15] W. Zimdahl and A.B. Balakin, *Class. Quantum Grav.* **15**, 3259 (1998).
 - [16] W. Zimdahl, D.J. Schwarz, A.B. Balakin and D. Pavón, *Phys. Rev. D* **64**, 063501 (2001).
 - [17] A.B. Balakin, D. Pavón, D.J. Schwarz and W. Zimdahl, *New J. Phys.* **5**, 85 (2003).
 - [18] A.B. Balakin, *Gen. Relat. Grav.* **36**, 1513 (2004).
 - [19] A. Balakin, R.A. Sussman and W. Zimdahl, *Phys. Rev. D* **70**, 064027 (2004).
 - [20] W. Zimdahl, D. Pavón and L.P. Chimento, *Phys. Lett. B* **521**, 133 (2001).
 - [21] W. Zimdahl and D. Pavón, *Gen. Relat. Grav.* **33**, 791 (2001).
 - [22] L.P. Chimento and D. Pavón, *Phys. Rev. D* **73**, 063511 (2006).
 - [23] N. Cruz, S. Lepe and F. Pena, *Phys. Lett. B* **663**, 338 (2008).
 - [24] J. Valiviita, E. Majerotto and R. Maartens, *JCAP*. **0807**, 020 (2008).
 - [25] O. Bertolami, F. Gil Pedro, M. Le Delliou, *Phys. Lett. B* **654**, 165 (2007).
 - [26] S. Nojiri and S.D. Odintsov, *Phys. Lett. B* **639**, 144 (2006).
 - [27] V.F. Cardone, C. Tortora, A. Troisi and S. Capozziello, *Phys. Rev. D* **73**, 043508 (2006).
 - [28] S. Nojiri and S.D. Odintsov, *Phys. Rev. D* **72**, 023003 (2005).
 - [29] I. Brevik, O.G. Gorbunova and A.V. Timoshkin, *Eur. Phys. J. C* **51**, 179 (2007).
 - [30] W. Chakraborty and U. Debnath, *Phys. Lett. B* **661**, 1 (2008).
 - [31] D. Jou, J. Casas- Vázquez and G. Lebon, *Extended Irreversible Thermodynamics* (Springer, Berlin, 1996).
 - [32] J.M. Stewart, *Non-equilibrium Relativistic Kinetic Theory* (Springer, New York, 1971).
 - [33] S.R. de Groot, W.A. van Leeuwen and Ch. G. van Weert, *Relativistic Kinetic Theory* (North Holland, Amsterdam, 1980).
 - [34] V. Sahni, T.D. Saini, A.A. Starobinsky and U. Alam, *JETP Lett.* **77**, 201 (2003); *Pisma Zh. Eksp. Teor. Fiz.* **77**, 249 (2003).
 - [35] V.G. Gurzadyan and R. Penrose, Concentric circles in WMAP data may provide evidence of violent pre-Big-Bang activity, arXiv: 1011.3706.
 - [36] L.P. Chimento, A.S. Jakubi, D. Pavon and W. Zimdahl, *Phys. Rev. D* **67**, 083513 (2003).
 - [37] S. Nojiri and S.D. Odintsov, *Phys. Lett. B* **637**, 139 (2006).
 - [38] H. Mohseni Sadjadi, M. Alimohammadi, *Phys. Rev. D* **74**, 103007 (2006).
 - [39] S. del Campo, R. Herrera and D. Pavon, *Phys. Rev. D* **78** 021302 (2008).
 - [40] G. Izquierdo and D. Pavon, *Phys. Rev. D* **70**, 084034 (2004).